ELSEVIER

Journal of Nuclear Materials 266–269 (1999) 406–411

journal of nuclear materials

Laboratory experiment on lithium chemistry and its application to effective wall conditioning

S. Kato *, M. Watanabe, H. Toyoda, H. Sugai

Department of Electrical Engineering, Nagoya University, Furo-cho, Chikusa-ku, Nagoya 464-8603, Japan

Abstract

Laboratory studies on the physical chemistry of lithium wall conditioning effects observed in fusion reactors are reported, focusing on a role of lithium in dramatic decrease in carbon impurities in TFTR. Auger depth analysis of lithium-deposited graphite shows deep intercalation of lithium into graphite at room temperature. Helium ion bombardment (150–200 eV) on the lithium-saturated graphite leads to preferential sputtering of lithium and reduction of the net sputtering yield of carbon by an order of magnitude. Finally, general precautions to achieve reproducible lithium effects in fusion machines are described.

Keywords: Lithium; Wall conditioning; Carbon impurities; TFTR

1. Introduction

Wall conditioning based on lithium deposition is characterized by the lowest Z material ($Z = 3$) used for the present-day conditioning, a variety of strong chemical activities, and a promising in situ technique in future fusion reactors [1]. Several methods have been used to introduce lithium into a plasma vessel: lithium pellet injection [2–7], vacuum evaporation of lithium from an oven [8–10], lithium crucible heating by scrape-off plasma [11], lithium borohydride discharge [12] and laser-controlled lithium aerosol [13]. A great success of lithium wall conditioning in TFTR has been reported since 1992, where deposition of a few milligrams of lithium on the bumper limiter leads to a considerable improvement of the energy confinement time from $\tau_E = 0.075$ s (L mode) to $\tau_E = 0.33$ s with very peaked density profiles [14].

Lithium wall conditioning effects appear as a very low hydrogen recycling (low edge density), reduction of oxygen impurity in a hot core plasma region, significant suppression of carbon impurity, and improvement of energy confinement. All these effects have been observed clearly in TFTR, however mixed results have been obtained on other machines (DIII-D, Alcator C-Mod, TdeV, JIPP TII-U, Heliotron E). Thus, there has been an open question why only TFTR could obtain the satisfactory results [1]. Moreover, fundamental studies have been needed to elucidate the underlying mechanisms leading to lithium effects.

The authors have been continuing basic laboratory studies of the physical chemistry of lithium effects since the 1988 first paper [8] proposing the lithium wall conditioning. Many chemical reactions of clean lithium surface with O_2, H_2O, CO and CH_4 were observed, together with hydrogen pumping and LiH formation [9,12,15]. These chemical activities of fresh lithium layer successfully account for the lithium effects observed in fusion machines, except for suppression of physical sputtering of graphite which has been thought to be a main source of carbon impurity in TFTR.

In this paper, a small-scale laboratory experiment supporting the considerable reduction of graphite sputtering in TFTR is reported with lithium–graphite intercalation compounds taken into account. In addition, general precautions to achieve the satisfactory lithium effects are described based on the laboratory studies on lithium chemistry.

* Corresponding author. Tel.: +81-52 789 4697; fax: +81-52 789 3150; e-mail: sugai@nuee.nagoya-u.ac.jp.

0022-3115/99/$ – see front matter
PII: S0022-3115(98)00889-7

2. Lithium-deposited graphite

In order to obtain information on the state of lithium deposited on graphite, in situ Auger analysis of various samples was carried out in a small device, Surface Modification Teststand (SUT) [16] in the National Institute for Fusion Science. Baking a lithium oven at ~500°C in vacuum gives rise to 100–300 nm thick lithium film on a graphite sample at room temperature. The film thickness is in situ estimated by a deposition monitor which is based on quartz crystal oscillation. The sample material is (i) isotropic graphite, IG-430U, Toyo Tanso which is used as the first wall material in JT-60U, (ii) strongly anisotropic pyrolytic graphite, Highly Oriented Pyrolytic Graphite (HOPG), and (iii) nickel as a reference of metal. All sample surfaces were polished with diamond powder.

After lithium deposition, the sample is transferred in vacuum, without exposing it to the air to an Auger analysis chamber. Typical examples of the measured depth profile are shown in Fig. 1 where ~10% oxygen involved during the analysis is deleted for simplicity. A remarkable difference between the nickel and the isotropic graphite is seen in Fig. 1(a,b): there is a 100 nm lithium layer on the nickel surface while, in case of graphite, no separate lithium layer is visible in spite of more lithium deposition (250 nm thick) but the graphite surface is composed of 60% carbon and 40% lithium. Such unusual distribution of lithium in graphite is contrast to graphite boronization: a separate boron layer of, say 100 nm thickness on a polished graphite surface is clearly observed in a test sample of JT-60U [17]. Thus, one can conclude that the unusual distribution is an evidence of *graphite intercalation compounds* where lithium atoms are inserted between the hexagonal layer planes [18].

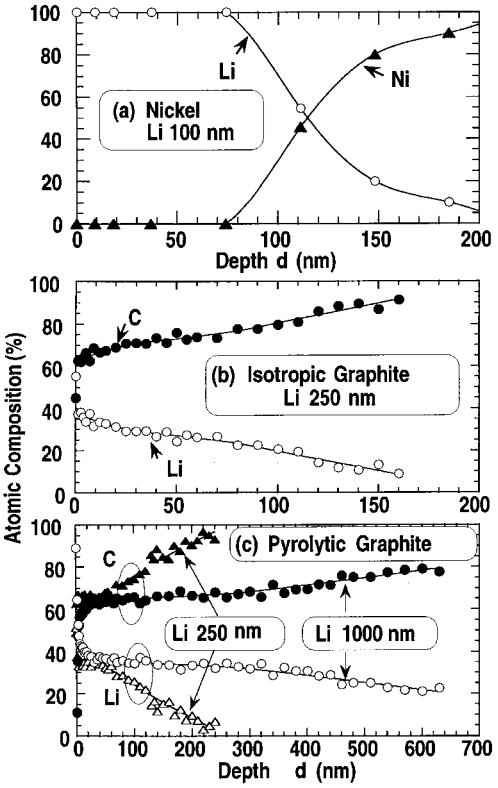

Fig. 1. Auger depth profile of lithium for (a) 100 nm Li deposition on nickel, (b) 250 nm Li deposition on isotropic graphite, and (c) 250 nm and 100 nm Li deposition on pyrolytic graphite (C: closed symbols, Li: open symbols)

Strictly speaking, the parameter of lithium thickness deposited on graphite, for example, 250 nm in Fig. 1(b), is meaningless since no lithium layer is actually formed on the graphite due to the intercalation. However, the lithium 'film' thickness is a convenient parameter indicating the amount of deposited lithium, and hence this parameter is used hereafter as well. Fig. 1(c) shows the depth profile for pyrolytic graphite (HOPG) where 'depth' means the distance *perpendicular* to the HOPG hexagonal plane. Comparison of the 250 nm data therein with the 250 nm data for the isotropic graphite [Fig. 1(b)] suggests that there is little difference in the depth profile of Li/C between the isotropic and the pyrolytic graphite. Even if a huge amount of lithium such as 1000 nm thick layer is deposited on the graphite, the lithium composition Li/(C + Li) does not increase but saturates at ~35% with deeper intercalation into the bulk, as seen in Fig. 1(c). In the saturated condition, the atomic ratio is Li/C ~ 1/2, so that the state can be expressed as LiC_2.

The observed saturation level of ~ 35% Li is rather high in comparison to conventional graphite intercalation compounds (GICs): the highest level of lithium content of the Li-GIC is 14%. In a field of lithium ion batteries in industry, about two times higher Li content (Li_2C_6) has been observed and the most condensed package structure is thought to be LiC_2 as measured in the present study. The limiting case is Li_2C_2 which is not the GIC but a covalent compound called lithium carbide [19] or lithium acetylide [20]. Any types of graphite (isotropic, pyrolytic, CFC) in fusion reactors are modified to amorphous carbon structures due to severe ion bombardment and redeposition. To simulate the lithium behaviors in such condition, amorphous carbon films were deposited on a silicon substrate, using the helium magnetron sputtering of graphite (see Section 3). After then, lithium was deposited on the amorphous carbon layer, which was followed by Auger surface analysis. Although the experiment is still preliminary, a separate lithium layer was not observed but lithium and carbon are mixed in the top layer of ~ 100 nm. Deep penetration of lithium in graphite such as ~20 μm has been observed in the analysis of graphite samples inserted in

DIII-D [21] and TFTR [22]. In TFTR, lithium ions (Li^-, Li^{2-}, Li^{3-}) are accelerated by the sheath voltage of ~200 V and S/CMS implanted to the high-temperature (>500°C) graphite limiter, so that lithium might penetrate into graphite more deeply than the present room-temperature thermal lithium experiment.

3. Physical sputtering of lithium-deposited graphite

3.1. Experimental

Sputtering yield of graphite was investigated using a dc magnetron sputtering device shown in Fig. 2, which enables high-flux ion bombardment on the graphite surface with the ion energies comparable to the bumper limiter bombardment in TFTR. A 13 cm diameter, 5 mm thick disk of isotropic (IG-430U) or pyrolytic (HOPG) is placed on a cathode which is water-cooled and biased to a negative voltage V_d (from −140 to −200 V) against a grounded anode. Let the origin ($r=0$, $z=0$) of cylindrical coordinate to be at the center of graphite surface disk. A donut-shape plasma of major radius $r \sim 4$ cm with the plasma potential of ~10 V is produced, typically at the discharge current $I_d = 0.12$. A in helium at 70 m Torr, under an axisymetric magnetic field (0.06T at $z=1$ cm, $r=4$ cm) which is generated by permanent magnets attached behind the cathode. Helium ion accelerated by a thin cathode sheath impinges on the graphite surface with kinetic energies of $\sim |eV_d|$, thus giving rise to sputtering mainly from a ring-belt region ($r=4$ cm, width $\Delta r=2$ cm).

The experimental procedure is as follows. Firstly, lithium beams effusing from the oven ($r=16.5$ cm, $z=11$ cm) is obliquely irradiated in vacuum on the graphite disk on the cathode, to deposit lithium layer. As inferred from the geometry shown in Fig. 2, the lithium deposition profile is rather nonuniform over the graphite disk. For example, the lithium thickness varies from 150 nm (bottom) to 65 nm (top) over the ring-belt sputtering region, and this case is referred as '100 nm' on average. The average thickness defined in this way can be estimated in situ using a deposition monitor at $r=26$ cm and $z=9.5$ cm. After lithium deposition, the lithium oven is closed by a shutter.

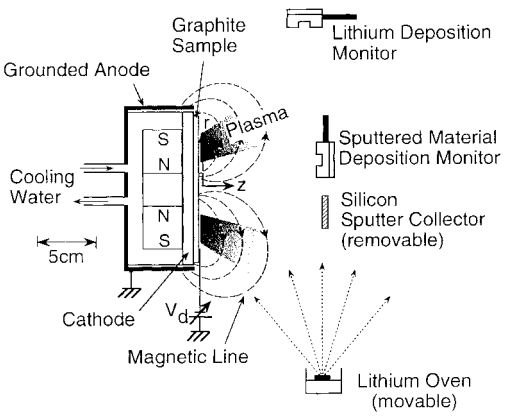

Fig. 2. Experimental setup for magnetron sputtering of lithium-deposited graphite.

Secondly, the magnetron discharge is ignited in helium and the helium ion bombardment induces physical sputtering of lithium-deposited graphite. The time variation of sputtering rate is indirectly measured by the second deposition monitor at $z=0$ and $r=11$ cm. This monitor is basically sensitive to the total mass deposited on the sensor, thus giving a measure of the sum of lithium and carbon masses sputtered from the graphite disk. Finally, a sputter collector of silicon substrate is set at the same position as the second deposition monitor, to collect the sputtered material and measure the atomic composition by Auger analysis.

3.2. Lithium effect on total sputtering yield

In the helium magnetron discharge, the lithium-deposited graphite is exposed to helium ion irradiation at ~200 eV which is typical energies of ions bombarding the graphite limiter in TFTR. The sputtered material is deposited on the deposition monitor placed 11 cm away from the graphite target. The measured deposition rate is thought to be proportional to the sputtering yield of the target. Fig. 3 shows the sputtering yield as a function

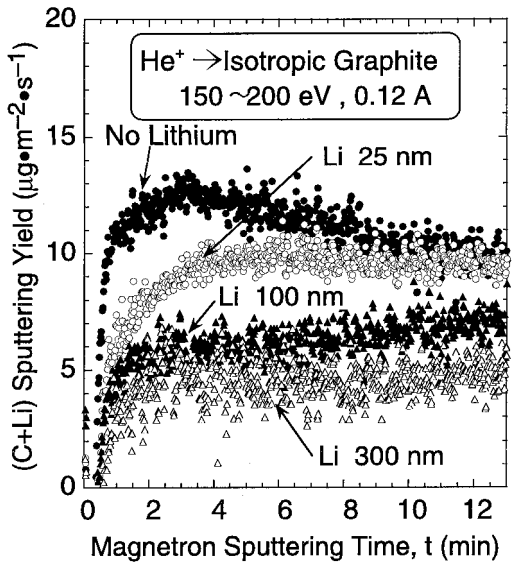

Fig. 3. Time variation of total (C + Li) sputtering yield with lithium dose as a parameter. Magnetron discharge (0.12 A, 140–200 V) in 70 m Torr helium.

of magnetron sputtering time in the case of isotropic graphite (IG-430U). Here the vertical scale and the unit ($\mu g m^{-2} s^{-1}$) do not denote the absolute sputtering yield of the target but the deposition rate measured on the monitor surface. The closed circles in this figure indicate the case without lithium deposition. A small amount (25 nm) of lithium deposition markedly reduces the sputtering yield for the initial 5 min discharge. With increasing the lithium dose, suppression of sputtering is more enhanced and lasts for longer time. The time scale of 10 min in the present experiment (ion fluence $\sim 10^{23}$ m^{-2}) corresponds to ~0.1 s in the tokamak edge plasma (ion flux $\sim 10^{24}$ m^{-2} s^{-1}). In tokamaks, however, the redeposition of lithium will make the lithium effect much longer.

In a course of the experiment, the discharge voltage V_d was observed to change at the constant current $I_d = 0.12$ A, depending on the lithium dose; for instance, $V_d \sim -140$ V at $\tau = 300$ nm while $V_d \sim -200$ V at $\tau = 0$. Such voltage change is attributed to a change in the secondary electron emission coefficient of the lithium-deposited graphite surface. Accordingly, the ion bombarding energy decreases from 200 eV for the pure graphite to 150 eV for the lithium-saturated graphite. When the helium ion energy is decreased from 200 to 150 eV, the sputtering rate of pure graphite becomes lower by ~20% [23]. Thus, the large decrease seen in Fig. 3 cannot be explained by the decrease in bombarding energy. Furthermore, it will be shown in the next section that most of sputtered material is not carbon but lithium.

The dependence of sputtering yield on the lithium dose is shown in Fig. 4 where the sputtering yields at $t = 2$ min in Fig. 3 are normalized by the value for no lithium and plotted as a function of the thickness r of deposited lithium 'film'. As seen in this figure, the sputtering yield decreases with increasing the lithium dose and becomes ~40% of the lithium-free graphite for $\tau > 100$ nm. The sputtering yield measured in this way is the *total sputtering yield as* the sputtered material contains both carbon and lithium.

3.3. Lithium effect on carbon sputtering yield

In order to discriminate the carbon sputtering yield from the total yield in Fig. 3 and Fig. 4, the atomic composition of sputtered material was investigated using the sputter collector (Fig. 2). First of all, 260 nm thick 'film' is deposited on isotropic graphite at room temperature and then the magnetron discharge ($I_d = 0.12$ A, $V_d \sim -140$ V) was turned on. The material sputtered during the first 20 min was deposited on the silicon substrate whose surface was in situ analyzed by Auger electron spectroscopy as shown in Fig. 5. Before sputtering, the graphite surface layer of ~100 nm thick is almost saturated with lithium at the level of ~30 at. % (Fig. 2(b)). If Li and C atoms should be sputtered at the same rate, then the deposited film on the silicon substrate would have ~70% C + ~30% Li. However, the sputtered material contains 15% C +85% Li, as shown in Fig. 5. This means that lithium is preferentially sputtered by ~150 eV helium ions. Such abundant lithium sputtering continues for 20 min or longer. This implies that lithium atom is successively supplied to the surface from the graphite bulk, probably because they can easily move in the intercalation layers. Thus, the top surface of graphite is thought to be always covered with plenty of lithium atoms during the sputtering, which prevents carbon atoms from bring sputtered.

Returning to Fig. 4, we can estimate the carbon sputtering yield for $\tau = 260$ nm, using the atomic composition (0.85 Li + 0.15 C) of sputtered material in Fig. 5. A straightforward calculation gives the carbon contribution to the total sputtering yield as $12.0 \times 0.15/$

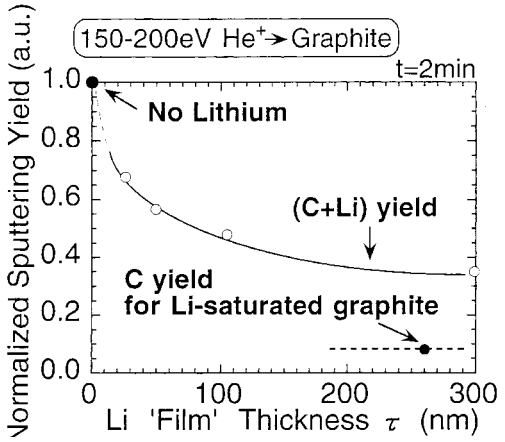

Fig. 4. Normalized sputtering yield at the sputtering time $t = 2$ min as a function of lithium dose expressed by film thickness τ. Closed circles denote C yield and (C + Li) yield, respectively.

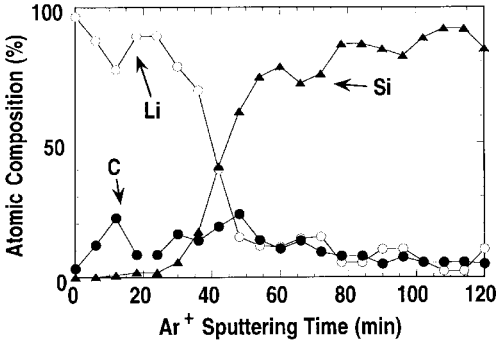

Fig. 5. Auger analysis of sputtered material collected on a silicon substrate during the magnetron sputtering (time $t = 0$–20 min).

$(12.0 \times 0.15 + 6.94 \times 0.85) = 0.234$ with the atomic mass taking into account. As a consequence, the carbon sputtering yield at $\tau = 260$ nm was found to be 0.08 when normalized by the yield for pure graphite, as plotted by a solid dot in Fig. 4. That is, the lithium deposition suppresses the physical sputtering yield by an order of magnitude. The preferential sputtering and rapid diffusion of lithium might make it difficult to explain the measured Auger depth profiles (Fig. 1). However, it is not obvious whether the lithium is preferentially sputtered by a high-energy (3 keV) heavy-ion (Ne^-) beam used in the Auger depth analysis. Another investigation is also needed to confirm that the lithium diffusion is slow enough to keep the as-received Li distribution in graphite unchanged during the Ne^- sputtering.

4. Precautions for lithium wall conditioning

Dramatic improvement of energy confinement time by a small amount of lithium deposition on the limiter has been observed in TFTR [14], along with suppression of hydrogen recycling, oxygen impurity, and carbon impurity. However, the lithium conditioning tested in other machines (DIII-D, JIPP TII-U, etc.) led to only marginal effects while no influence was recognized in Alcator C-Mod. This situation is contrast to boronizations which have given almost same effects in all machines In this section, we discuss the origin of different results in different machines in lithium conditioning, and describe general precautions to achieve satisfactory lithium effects.

Table 1 summarizes the lithium effects observed in fusion machines and the underlying physical chemistry disclosed in the laboratory studies [8,9,12,15]. Although not shown in this table, lithium reacts with metal oxides to reduce them, forming lithium oxide (Li_2O). This might be the reason why the full metal machine Alcator C-Mod had no influence of lithium pellet injection. There would have appeared the lithium effect even in Alcator C-Mod if a plenty of lithium had been deposited on the metal wall.

It should be noted that a lifetime of lithium atom is very short due to its strong chemical reactivity (this is not the case in boronization). For example, lithium reacts with most of residual gases (H_2O, O_2, CO and CH_4) in fusion devices through the reactions (ii)–(iv) in Table 1. One can easily calculate that monolayer of lithium is killed by a background water vapor at 10^{-9} Torr. Furthermore, hydrogen atoms involved in graphite walls react with deposited lithium through the reaction (i), forming lithium hydride (LiH). If such reaction should take place and lithium atom be totally consumed there, no further hydrogen pumping would be expected in the next main shot. Thus, a key point to reduce the hydrogen recycling is to keep free lithium atoms on the wall as many as possible prior to main discharges. The amount *of free* lithium atom should be equal to or larger than the total hydrogen fluence to the wall during the main discharge, for single Li atom captures single H atom in the reaction (i).

Accordingly, general precautions to obtain reproducible lithium effects in fusion experiments are summarized as follows.

1. *Reduce background oxygen impurities* such as metal oxides and oxygen containing gases (H_2O, O_2, CO etc.). Otherwise, clean lithium surface will be invaded by residual gases between the discharge shots.
2. *Reduce the hydrogen retention in graphite walls.* If the graphite contains lots of hydrogens in the bulk, lithium deposited on the graphite will intercalate and react with hydrogen to form LiH: such bounded lithium does not capture hydrogen anymore. One of the key techniques used in TFTR was to reduce the hydrogen retention of graphite by ohmic helium discharges.
3. *Deposit sufficient amount of lithium* prior to main discharges. As mentioned above, the lithium dose should exceed the total hydrogen fluence during the main discharges, to obtain the low hydrogen recycling.

Table 1
Lithium wall conditioning effects and related physical chemistry

Lithium effects	Lithium physical chemistry	
Hydrogen pumping (*Suppression of H recycling*)	$Li + H \rightarrow LiH$ (H^+)	(i)
Residual gas pumping	$2Li + O_2 \rightarrow 2Li_2O$	(ii)
(*Suppression of O impurity*)	$2Li + 2H_2O \rightarrow 2LiOH + H_2$ ($2LiOH \cdot H_2O$)	(iii)
(*Suppression of C impurity*)	$4Li + 3CO \rightarrow Li_2CO_3 + Li_2C_2$	(iv)
Modification of graphite (*Suppression of C sputtering*)	$Li + nC_6 \rightarrow LiC_{6n} (n = 1, 2, \cdots), LiC_2$ Intercalation of lithium into bulk graphite	(v)

5. Summary and conclusions

The previous laboratory studies on lithium conditioning effects [8,9,12,15] revealed a variety of chemical reactions of lithium with hydrogen and residual gases (H_2O, O_2, CO etc.) which account for the observed suppression of hydrogen recycling and oxygen impurity. As far as carbon impurity is concerned, 25% reduction of chemical sputtering of graphite has been observed [12]. In this paper, the mechanism of decrease in physical sputtering of graphite is presented, with a carbon impurity decrease in TFTR in mind.

Auger depth profile measurements clearly show the intercalation of lithium into graphite at room temperature and the lithium content saturation at ~35%. Magnetron sputtering studies on the lithium-saturated graphite demonstrated preferential lithium sputtering (85% Li + 15% C) and a dramatic reduction of net carbon sputtering yield (~1/10 of that without lithium deposition) at 150–200 eV helium ion bombardment. A series of laboratory experiments on lithium chemistry suggest the need of careful preparation for the well-defined lithium conditioning. Three precautions to obtain the lithium effects are described: reduce the background oxygen impurities, reduce the hydrogen retention in graphite and deposit sufficient amount of lithium.

Acknowledgements

This work was partly carried out under the Collaborating Research Program at the National Institute for Fusion Science, and under a Personnel Exchange Program, the Japan–US Cooperative Research Program. The authors would like to thank the NIFS group (K. Tsuzuki, A. Sagara, N. Noda) and the Princeton group (C.H. Skinner, D.K. Mansfield, H.W. Kugel) for valuable discussions and comments. They also thank Dr T. Tanabe for useful information on graphite intercalation compounds, and Toyo Tanso Co. for supplying graphite materials.

References

[1] J.T. Hogan, C.E. Bush, C.H. Skinner, Nucl. Fusion 37 (1997) 705.
[2] J.A. Snipes et al., J. Nucl. Mater. 196–198 (1992) 686.
[3] D.K. Owens et al., J. Nucl. Mater. 220–222 (1995) 62.
[4] D.K. Mansfield et al., Phys. Plasmas 3 (1996) 1892.
[5] K.M. McGuire et al., Phys. Plasmas 2 (1995) 2176.
[6] G.L. Jackson et al., J. Nucl. Mater. 241–243 (1997) 655.
[7] K. Kondo et al., J. Nucl. Mater. 241–243 (1997) 956.
[8] T. Isozumi, S. Yoshida, H. Sugai, Kaku Yugo Kenkyu 60 (1988) 304.
[9] H. Sugai, H. Toyoda, K. Nakamura, K. Furuta, M. Ohori, K. Toi, S. Hirokura, K. Sato, J. Nucl. Mater. 220–222 (1995) 254.
[10] H.W. Kugel, J. Gorman et al., in: 17th IEEE/NPSS Symp. on Fusion Engineering (October 1997, San Diego).
[11] B. Terreault et al., J. Nucl. Mater. 220–222 (1995) 790.
[12] H. Toyoda, M. Watanabe, H. Sugai, J. Nucl. Mater. 241–243 (1997) 1031.
[13] D.K. Mansfield et al., private communications.
[14] C.H. Skinneret et al., J. Nucl. Mater. 241–243 (1997) 214.
[15] H. Sugai, M. Ohori, H. Toyoda, Vacuum 47 (1996) 981.
[16] N. Noda, A. Sagara et al., J. Nucl. Mater. 220–222 (1995) 623.
[17] M. Saidoh, N. Ogiwara et al., Jpn. J. Appl. Phys. 32 (1993) 3276.
[18] S.A. Solin, H. Zabel, Adcance in Phys. 37 (1988) 87.
[19] H. Kubo, C.H. Wu, J. Nucl. Mater. 201 (1993) 261.
[20] M. Asano, K. Kubo, J. Nucl. Mater. 102 (1981) 353.
[21] G.L. Jackson, R. Bastasz et al., presented at the Workshop on Lithium Effects in Plasmas, Oct. 17–18, 1996, Princeton.
[22] Y. Hirooka, K. Ashida et al., presented in 13th Int. Conf. on Plasma–Surface Interactions, San Diego, May 18–22, 1998.
[23] J. Roth, in: D.E. Post, R. Behrish (Eds.), Physics of Plasma–Wall Interactions in Controlled Fusion, Plenum, New York, 1984, p. 360.